Marine and Petroleum Geology 26 (2009) 1190–1198

Contents lists available at ScienceDirect

Marine and Petroleum Geology

journal homepage: www.elsevier.com/locate/marpetgeo

Petrographic and geochemical characterization of seep carbonate from Bush Hill (GC 185) gas vent and hydrate site of the Gulf of Mexico

Dong Feng [a,c], Duofu Chen [a,*], Harry H. Roberts [b]

[a] CAS Key Laboratory of Marginal Sea Geology, Guangzhou Institute of Geochemistry, Chinese Academy of Sciences, 511 Kehua Street, Wushan, Guangzhou 510640, China
[b] Coastal Studies Institute, Louisiana State University, Baton Rouge, LA 70803, USA
[c] Graduate University of Chinese Academy of Sciences, Beijing 100049, China

ARTICLE INFO

Article history:
Received 23 January 2008
Received in revised form 19 June 2008
Accepted 1 July 2008
Available online 6 July 2008

Keywords:
Seep carbonate
Carbon and oxygen stable isotopes
Rare earth elements
Redox variation
Bush Hill
Gulf of Mexico

ABSTRACT

Authigenic carbonates are common at cold seep sites as a result of microbial oxidation of hydrocarbons. Seep carbonate samples were collected from the surface of the Bush Hill (Green Canyon Block 185, Gulf of Mexico), a mound containing gas hydrate. The carbonates consisted of oily, porous limestone slabs and blocks containing bioclasts and matrix. Analysis by X-ray diffraction shows that aragonite is the dominant mineral (89–99 wt% with an average of 94 wt%) in the matrix of seep carbonate. This cement occurs in microcrystalline, microspar, and sparite forms. The moderate ^{13}C depletion of the seep carbonate (the most depleted one has $\delta^{13}C$ value of $-29.4‰$, and 26 of 38 subsamples have $\delta^{13}C$ values $>-20.0‰$) indicates that the non-methane hydrocarbons was incorporated during seep carbonate precipitation. Relative enrichment of ^{18}O may be related to localized destabilization of gas hydrate or derived from ^{18}O-enriched pore water originated from smectite–illite transition in the deep sediments. The total content of rare earth elements (REE) of the 5% HNO_3-treated solution of the carbonates is from 0.40 ppm to 30.9 ppm. The shale-normalized REE patterns show varied Ce anomalies from significantly negative, slightly negative, and no to positive Ce anomalies. Variable content of trace elements, total REE, and Ce anomalies in different samples and even in the different carbonate mineral forms (microcrystalline, microspar and sparite) of the same sample suggest that the formation condition of the Bush Hill seep carbonate is variable and complex, which is possibly controlled by the rate of fluid flux.

1. Introduction

Seep carbonate precipitation is a widely observed phenomenon in the modern and ancient marine seep environments of the world (Roberts and Aharon, 1994; Peckmann et al., 2001; Peckmann and Thiel, 2004; Campbell, 2006; Naehr et al., 2007). Carbonate precipitation at hydrocarbon seep sites is a result of microbial oxidation of methane, as well as higher molecular weight hydrocarbons, through the combined metabolism of methane oxidizing archaea (MOA) and sulfate reducing bacteria (SRB) (Hinrichs et al., 1999; Boetius et al., 2000; Valentine and Reeburgh, 2000; Michaelis et al., 2002). The minerals in seep carbonate are mainly Mg-calcite, aragonite, and dolomite (Hovland et al., 1987; Roberts and Aharon, 1994; Peckmann et al., 2001; Naehr et al., 2007). The chemo-physical factors controlling the mineralogy in seep carbonates are still not well understood (Peckmann et al., 2001). It is obvious that at seepage sites, the precipitation of aragonite is promoted over calcite when high sulfate concentration occurs (Aloisi et al., 2000).

The carbon isotopic composition of seep carbonate serves as an indicator of the carbon sources incorporated during carbonate precipitation because the carbonates inherit the stable carbon isotopic signature from the carbon sources present in the seeps (Roberts and Aharon, 1994; Peckmann et al., 2001; Peckmann and Thiel, 2004). The $\delta^{18}O$ values, on the other hand, provide information pertaining to the temperature and fluid source from which seep carbonate is precipitated (e.g. Naehr et al., 2000). Additionally, due to the enrichment of ^{18}O in gas hydrates, anomalously positive $\delta^{18}O$ of seep carbonate could argue in favor of gas hydrate destabilization at seep sites (Bohrmann et al., 1998; Aloisi et al., 2000, 2002; Greinert et al., 2001; Peckmann and Thiel, 2004; Chen et al., 2005). However, the smectite-illite transition in the deep sediments can also generates ^{18}O-enriched pore water which could provide a source of ^{18}O-enriched pore water for carbonate precipitation (Hesse, 2003).

The behavior of rare earth elements (REE) has been widely reported in hydrothermal carbonate deposits (Barrat et al., 2000) and in carbonate of the normal marine environments, like coral (Sholkovitz and Shen, 1995). However, there has been relatively little investigation of the behavior of trace elements, especially REE, from hydrocarbon seep carbonates.

* Corresponding author. Tel.: +86 20 8529 0286; fax: +86 20 8529 0130.
E-mail addresses: fd@gig.ac.cn (D. Feng), cdf@gig.ac.cn (D. Chen), hrober3@lsu.edu (H.H. Roberts).

0264-8172/$ – see front matter © 2008 Elsevier Ltd. All rights reserved.
doi:10.1016/j.marpetgeo.2008.07.001

Bush Hill is one of the most studied areas for gas hydrate and hydrocarbon seeps in the world. Seep communities, authigenic carbonate, gas and oil seeps, and gas hydrates are common on the surface of seafloor (MacDonald et al., 1989, 1994; Roberts and Aharon, 1994; Sassen et al., 2004; Tryon and Brown, 2004). Previous research has shown that vent gas and hydrate gas derives from thermogenic gas that migrated to seafloor from the subsurface petroleum system (Jolliet reservoir) (e.g. Chen and Cathles, 2003; Chen et al., 2004; Sassen et al., 2003, 2004). Some seep carbonate samples collected from the Bush Hill site display extremely negative $\delta^{13}C$ values (−55‰ to −40‰), and thereby have been considered to favor a methane carbon source (Roberts and Aharon, 1994). However, additional data from recent investigations show that the majority of sulfate reduction at the Bush Hill sites is likely fueled by the oxidation of organic matter, possibly heavier hydrocarbons (C_{2+}) like oil, rather than methane (Joye et al., 2004). Moreover, the measurement of gas and water flux and chemical analyses show large degrees of spatial and temporal variability of vent rate and fluid sources in this region (Roberts et al., 1999; Roberts, 2001; Leifer and MacDonald, 2003; Chen et al., 2004; Tryon and Brown, 2004).

In this study, we have investigated sedimentary structure and mineralogy, stable carbon and oxygen isotope, REE, and trace elements of the seep carbonate collected at Bush Hill. We provide evidence that the formation conditions of the seep carbonates are highly variable and complex, and the fluid flow rate at this hydrocarbon seep site may be the primary factor controlling the formation conditions of the authigenic carbonates and their variable geochemical characteristics.

2. Sampling and analytical methods

Bush Hill (27°46′ N; 91°30′ W) is a fault-related seep and hydrate site located near the boundary of GC 184 and GC 185, Gulf of Mexico, where water depth is ~540 m (Fig. 1), and the average bottom water temperature is ~7 °C. The seep carbonates described here were collected in 1997 and 1998 during the Johnson-Sea-Link I (JSL I) manned submersible dives 2904, 4061 and 4063 using the robot arm of the submersible (Table 1).

Petrographic observation of thin sections of the samples was made using a LEICA-DMRX optical microscope with Leica Qwin Program. The microstructure of the seep carbonate on the fresh surfaces of fractured samples was examined with a scanning electron microscope (SEM). The samples were prepared by gold coating to a thickness of ~200 Angstroms for the SEM observations. Photographs were taken using a Sirion 200 FE-SEM equipped with EDAX GENESIS. For X-ray diffraction (XRD), the samples were crushed into powder less than 200 mesh using an agate mortar and pestle. The XRD analyses were performed using a Rigaku DXR 3000 computer-automated diffractometer utilizing Bragg–Brentano geometry. The X-ray source was a Cu anode operated at 40 kV and 40 mA using CuKα radiation equipped with a diffracted beam graphite monochromator. The orientated samples were scanned at an interval of 5–65° (2θ) with a step size of 0.02° and count time of 5 s per step. Divergence, scattering, and receiving slits were 0.5°, 0.5° and 0.15 mm, respectively. Relative abundance of the minerals was semi-quantified by Rietveld analysis of the diffractograms with the program SIROQUANT (Taylor, 1991).

The powdered samples were processed with 100% phosphoric acid to release CO_2 for stable carbon and oxygen isotope analysis. Carbonate carbon and oxygen isotopic compositions in permil (‰) relative to PeeDee Belemnite (PDB) standard were measured by using the GV Isoprime II stable isotopic mass spectrometry with deviations less than 0.01‰ (2σ) for both $\delta^{18}O$ and $\delta^{13}C$ values.

The seep carbonate powder (0.1–0.5 g) was treated with 50 ml of 5% HNO_3 in a centrifuge tube for 2–3 h to separate the carbonate mineral phase and residue phase. Then, 2500 ng of Rhodium was added as an internal standard for calculating the element concentration of dissolved carbonate mineral phase. Five milliliters of this solution was further diluted 10 times to be used for the REE and trace elements analysis by using Finnigan MAT ELEMENT high

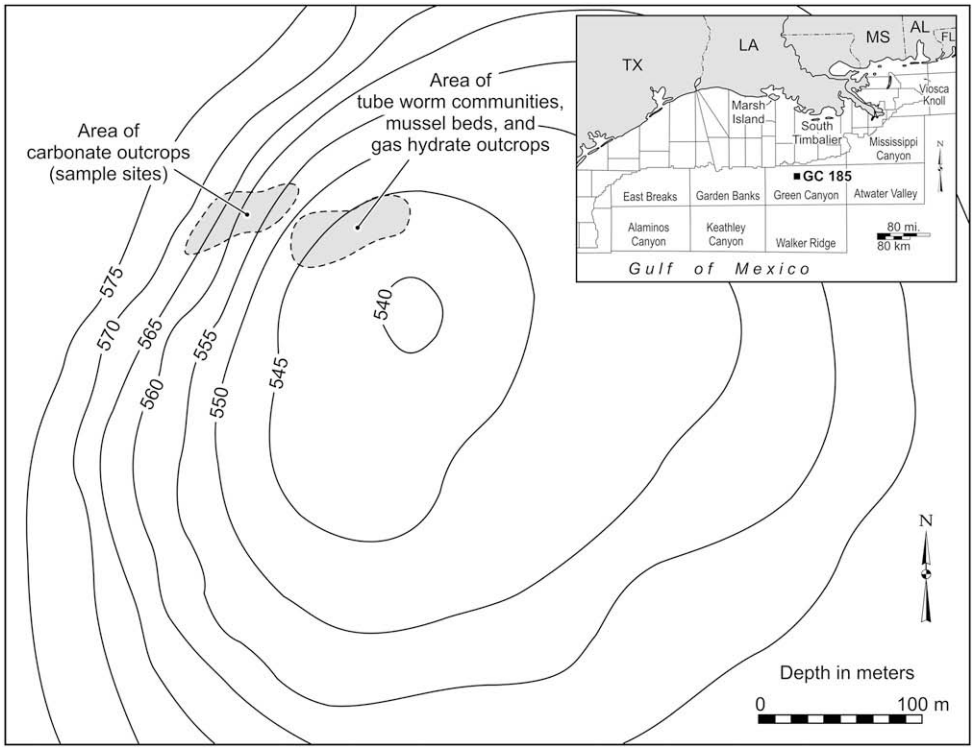

Fig. 1. Bathymetric map of the Bush Hill study site, showing the area of carbonate outcrops, where the samples were collected, and the area of tube worm communities, mussel beds, and gas hydrate outcrops. Small black solid-square in the middle of the insert is the location of the Bush Hill mound.

Table 1
Samples collection information and mineral composition of Bush Hill seep carbonates based on X-ray diffraction

Sample number	Year-Dive number	Relative percentages (wt%)				
		Aragonite	Calcite	Muscovite	Kaolinite	Dolomite
BH-A	1997-JSL I-2904	94.9	5.10	<0.1	–	–
BH-B	1997-JSL I-2904	88.5	3.80	4.8	1.7	–
BH-C	1997-JSL I-2904	99.0	0.90	0.1	–	–
BH-D	1997-JSL I-2904	99.1	0.90	–	–	–
BH-F	1998-JSL I-4061	97.1	2.90	–	–	–
BH-G	1998-JSL I-4063	92.5	7.50	–	–	–
BH-H	1998-JSL I-4063	88.7	3.30	–	–	7.8

resolution ICP-MS. Precision of the REE and trace element analysis was checked by multiple analyses of international carbonate standard samples CAL-S. The average standard deviations are less than 10%, and average relative standard deviations are better than 5%. For the detail of ICP-MS analysis see Qi and Gregoire (2000) and Qi et al. (2005).

3. Petrography

The authigenic carbonate samples occur as solidified to semi-solidified crusts from grey, white to grey, yellow in color with variable porosity. Tube worm casts, serpulid wormtubes, and microbial degraded crude oil are present (Fig. 2). Lucinid-vesycomyid clam shells, up to 9.5 cm in length and 4.5 cm in width, are well preserved in the carbonates. This single type of bivalve shell occurs as imbricate structure, and is the volumetrically dominant component (>40% in volume) in some samples (Fig. 2).

The XRD analysis of carbonate matrix shows that aragonite is the most abundant mineral (89–99 wt%, average 94 wt%), with minor amounts of calcite and dolomite (Table 1). Samples BH-C and BH-D contain the most aragonite. However, samples BH-A, BH-B, BH-F, BH-G, and BH-H seem to contain much more calcite, and BH-B has some portion of clay minerals (muscovite and kaolinite) whereas other samples are pure in aragonite and calcite. Pyrite was also observed under optical microscope and SEM (Figs. 3 and 4).

Aragonite occurs in microcrystalline, microspar, and sparite forms in the carbonate sample (Fig. 3A and B). The microcrystalline aragonite is black to grey in color under binocular, <5 μm and mostly ~1 μm in diameter. Some microcrystalline crystals were recrystallized or partially recrystallized to form microspar from 5 μm to 20 μm in diameter. The sparite crystals usually, up to 0.6 mm in length, form multiple layers in the botryoidal cements (Fig. 3B).

Pyrite framboids, aragonite clotted microfabrics, and botryoidal cements were observed in the seep carbonate (Figs. 3 and 4). Pyrite framboids, ~5–10 μm in diameter (average ~7 μm) are dispersed within seep carbonates, and they also occurs within the foraminifer chambers. The framboids are composed of numerous smaller particles, ~0.5 μm in diameter, and mostly occurring as cubic or pentagonal dodecahedron crystals (Fig. 4). Clotted microfabrics with misty borderline <100 μm in diameter are the aggregates of microcrystalline aragonite (Fig. 3C). These aggregates generally show an intense fluorescence. Botryoidal cements consist of fibrous aragonite crystals, usually arising from a dark nuclear mass. This type of cement commonly occurs as an isopachous layer showing multiple stages of growth (Fig. 3B), or it fills voids up to 0.5 mm in diameter.

4. Geochemistry

4.1. Isotope geochemistry

Stable isotopes of carbon and oxygen were measured on the different components of seep deposits, including microcrystalline aragonite, microspar aragonite, sparite aragonite, bivalve shells, and serpulid worm tubes (Table 2 and Fig. 5). The results show that the carbon and oxygen isotopic values of the Bush Hill seep carbonates can be divided into three groups (Fig. 5). Group I has relatively depleted ^{13}C ($\delta^{13}C$: −29.4‰ to −15.1‰) and enriched ^{18}O ($\delta^{18}O$: 2.4‰ to 5.0‰) as shown by all microcrystalline aragonite samples, eight microspar aragonite samples, and five sparite aragonite samples. Group II has relatively enriched ^{13}C ($\delta^{13}C$: −10.6‰ to −1.4‰) and ^{18}O ($\delta^{18}O$: 3.1‰ to 4.5‰) shown by all bivalve shell and serpulid worm tubes samples, one sparite aragonite sample and two microspar aragonite samples. Group III has relatively enriched ^{13}C ($\delta^{13}C$: −8.0‰ to −2.7‰) and depleted ^{18}O ($\delta^{18}O$: −0.6‰ to 0.3‰) as represented by eight microspar aragonite samples (Table 2 and Fig. 5).

4.2. Trace element geochemistry

The results of trace element analysis are listed in Table 3. The REE content is 7.07–26.57 ppm for microcrystalline aragonite, 0.40–3.10 ppm for microspar aragonite, 0.85–2.38 ppm for sparite aragonite, and 1.65–30.86 ppm for bivalve shells. The REE content of microcrystalline aragonite is higher than that of sparite aragonite and microspar aragonite in the same sample (Table 3). The shale-normalized REE patterns of seep deposits exhibit negative Ce anomalies ($Ce/Ce^* < 0.95$, e.g. samples BH-C and BH-D), no Ce anomalies ($0.95 < Ce/Ce^* < 1.05$, e.g. sample BH-H), and positive Ce anomalies ($Ce/Ce^* > 1.05$, bivalve shell in sample BH-G) (Table 3). The Ce anomaly of microcrystalline aragonite is more negative than that in sparite and microspar aragonite in the same sample (Fig. 6 and Table 3).

Strontium contents in microcrystalline aragonite are from 5168 ppm to 9147 ppm, except for sample BH-H which has low Sr content (94 ppm). The Sr concentrations vary from 2490 ppm to 9054 ppm in microspar aragonite, 8787 ppm to 9206 ppm in sparite aragonite, 113 ppm to 2624 ppm in bivalve shells. Barium contents in microcrystalline aragonite samples range from 17 ppm to 93 ppm although sample BH-H has a very high content (902 ppm). Barium contents are 10 and 19 ppm in the two microspar aragonite samples, 15 ppm and 26 ppm in the two sparite aragonite samples, 12 ppm and 55 ppm in the two bivalve shell samples (Table 3). Elements V, Mo, U, and Cd contents are highly variable, however, it appears that the higher contents are more likely in the microcrystalline aragonite than in the microspar and sparite aragonite.

5. Discussion

5.1. Hydrocarbon-derived carbonate

5.1.1. Carbon and oxygen stable isotopes

The $\delta^{13}C$ value of methane in the Gulf of Mexico is from −120‰ to −30‰ (Sackett, 1978; Whiticar et al., 1986), crude oil is averaging −25‰ (Roberts and Aharon, 1994), and seawater CO_3^{2-} is 0 ± 3‰ (Anderson and Arthur, 1983). The carbon and oxygen isotopes of the Bush Hill seep carbonates can be divided into three groups (Fig. 5). Group I has moderate depletion $\delta^{13}C$ values from −29.4‰ to −15.1‰ in the microcrystalline, sparite, and microspar aragonite (Table 2 and Fig. 5). These moderately depleted $\delta^{13}C$ values could be derived from non-methane hydrocarbons, probably the microbial degradation of crude oil. These values are also supported by the frequent occurrences of biodegraded crude oil in the pores of carbonate samples (Fig. 2). Based on a carbon isotope mass balance model (Formolo et al., 2004), the seep carbonate carbon source at the Bush Hill is mainly from non-methane hydrocarbons and only minor carbon has been contributed from methane, which is consistent with the previous results (Joye et al., 2004).

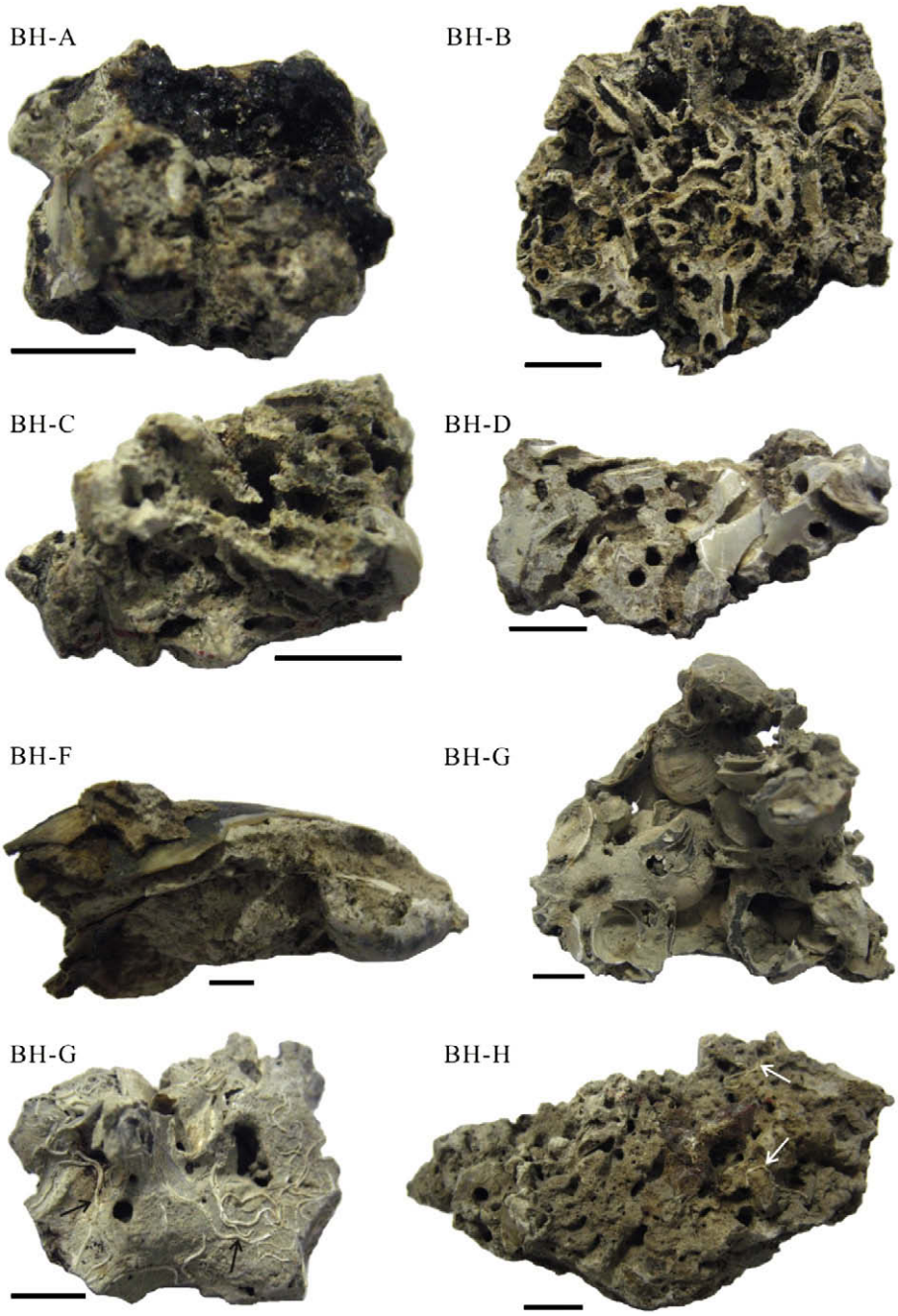

Fig. 2. Morphology of seep carbonate from Bush Hill mound. BH-A, asphalt (upper right part) within carbonate; BH-B, large amount of warm tubes preserved in seep carbonate; BH-C and BH-D, porous carbonate; BH-F: lucinid-vesycomyid clam shells up to 9.5 cm length and 4.5 cm width in seep carbonate; BH-G, single type of bivalve shell occurs as imbricate structure; BH-H, occurrence of the microbial degradation of crude oil in seep carbonate, Serpulid worm tubes (arrows) attached on its surface. Allscale bars = 1 cm.

In contrast, the $\delta^{13}C$ values of Group II shown by the shells and small worm tubes are from −10.6‰ to −1.4‰ (Fig. 5 and Table 2), much less ^{13}C-depleted than that of Group I, which is similar to the $\delta^{13}C$ values of tube worms and chemosymbiotic shells reported by Roberts and Aharon (1994) and Aharon et al. (1997). Two samples of microspar and one sample of sparite have similar values (Fig. 5). These higher $\delta^{13}C$ values of Group II are possibly the mixed source of seawater ($\delta^{13}C = 0 \pm 3$‰, Anderson and Arthur, 1983) and non-methane hydrocarbons, such as oil ($\delta^{13}C = -28$‰ to −25‰, Aharon et al., 1997). The microspar aragonite in Group III has similar $\delta^{13}C$ values (−8.0‰ to −2.7‰) with the Group II (Fig. 5). The microspar aragonite is partially recrystallized from microcrystalline aragonite. Thus, the carbon source of microspar aragonite may be inherited from the carbon of microcrystalline aragonite but modified by recrystallization in later diagenesis.

The oxygen isotopic composition of authigenic carbonate is controlled by a combination of factors including: (1) sample mineralogy and chemistry, (2) temperature of carbonate precipitation, and (3) pore fluid isotopic composition (Anderson and Arthur, 1983). Aragonite at Bush Hill precipitated in equilibrium with bottom water ($\delta^{18}O$ is about 0.7‰ V-SMOW) at 7 °C has a $\delta^{18}O_{PDB}$ value of approximately 3.67‰, according to Hudson and Anderson (1989). The $\delta^{18}O$ ratios of Groups I and II carbonates are from 2.44‰ to 4.96‰. Most of them fall into the range of 3–4‰ (Table 2), indicating that they are likely precipitated from fluids at ambient bottom water temperature. However, Group III has the

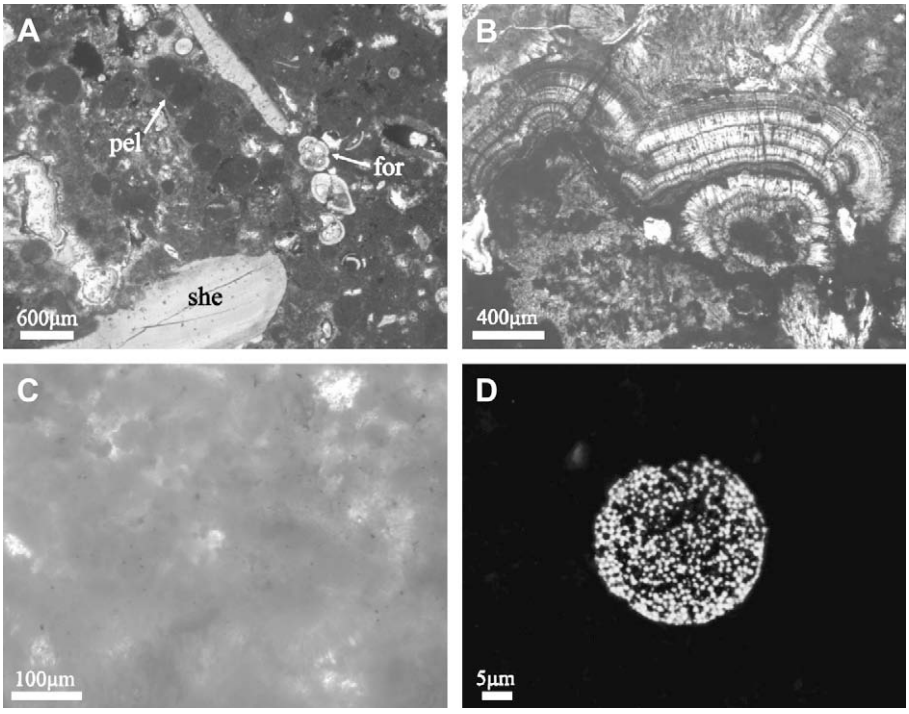

Fig. 3. The microscopic images of seep carbonate from Bush Hill. (A) Matrix has peloid (labeled "pel"), foraminifer (labeled "for"), and bivalve shell (labeled "she"), plane-polarized light; (B) sparite aragonite occurs as isopachous layer, plane-polarized light; (C) clotted microfabric has irregular shape and unclear margin, plane-polarized light; (D) framboidal pyrite consists of numerous small particle of pyrite (white) and aragonite (black) grains, reflected light.

$\delta^{18}O$ ratios that range from −0.58‰ to 0.35‰, indicating an equilibrium temperature from 21.4 °C to 25.5 °C, higher than ~7 °C of normal bottom water temperature. Measured bottom water temperature at Bush Hill gas vent site could be up to 10 °C (Roberts et al., 1999; MacDonald et al., 2005) and even over 20 °C (Roberts, 2001) at active vents, suggesting that these lower $\delta^{18}O$ ratios result from the effect of higher temperature which is most probably related to the expulsion of warm fluids at seafloor because of the rapid flux. These warm fluids may result in the recrystallization of microcrystalline aragonite.

In addition, some samples in the Group I have even higher $\delta^{18}O$ ratios (up to 4.96‰). The smectite–illite transition generates ^{18}O-enriched pore water, and the advection of such pore water along migration pathways to seafloor vent sites would provide a source of ^{18}O-enriched water for carbonate precipitation (Hesse, 2003). On the other hand, gas hydrate preferentially incorporates heavier oxygen isotopic water during crystallization (Davidson et al., 1983; Matsumoto, 2000). Therefore gas hydrate decomposition liberates water enriched in ^{18}O about 1–2.9‰ (Hesse and Harrison, 1981). The ongoing dissolution/decomposition of gas hydrates was

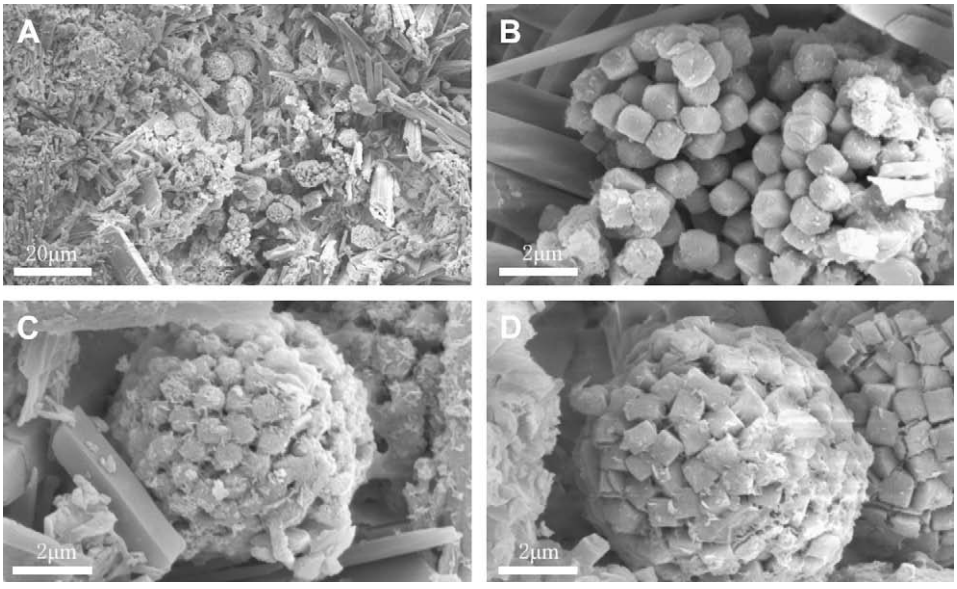

Fig. 4. SEM images of pyrite framboids. (A) Pyrite framboids ~5–10 μm in diameter dispersed within seep carbonates. The framboids are composed of numerous smaller particles, ~0.5 μm in diameter, and mostly occurring as pentagonal dodecahedron (B), spheric (C), and cubic (D) crystals. Very small filaments <0.1 μm in diameter on the pyrite surface are unknown, and may be clay mineral or bacteria.

Table 2
Carbon and oxygen stable isotopes of seep deposits from Bush Hill (‰, PDB)

Number	Type[a]	$\delta^{13}C$	$\delta^{18}O$	Number	Type[a]	$\delta^{13}C$	$\delta^{18}O$
BH-A	mi	−21.37	4.96	BH-F	bi	−2.96	3.33
BH-A	ms	−24.52	3.38	BH-F	bi	−1.68	3.62
BH-A	ar	−29.41	3.56	BH-F	swt	−1.39	3.30
BH-A	ms	−19.65	3.76	BH-F	mi	−22.79	3.30
BH-B	mi	−24.17	3.10	BH-F	ms	−25.28	3.35
BH-C	mi	−20.05	3.54	BH-F	ar	−27.59	3.17
BH-C	ms	−19.56	3.41	BH-F	ms	−27.94	3.22
BH-C	ar	−19.87	4.34	BH-G	bi	−10.56	3.15
BH-C	ms	−5.01	−0.35	BH-G	bi	−5.58	3.17
BH-C	ms	−7.99	0.35	BH-G	swt	−1.55	3.26
BH-D	ms	−5.64	−0.58	BH-G	mi	−26.95	3.59
BH-D	ms	−5.33	−0.35	BH-G	ms	−24.18	3.24
BH-D	mi	−15.13	2.44	BH-G	ms	−27.12	3.32
BH-D	ms	−4.30	−0.03	BH-H	mi	−17.93	3.84
BH-D	ms	−5.04	−0.21	BH-H	ms	−15.35	3.60
BH-D	ar	−16.51	4.04	BH-H	ar	−4.05	3.34
BH-D	ms	−2.70	0.31	BH-H	ar	−15.19	3.72
BH-D	ms	−4.18	0.53	BH-H	ms	−5.05	3.39
BH-F	bi	−6.00	3.62	BH-H	ms	−6.41	3.45

[a] mi, microcrystalline aragonite; ar, sparite aragonite; ms, microspar aragonite; bi, bivalve shell; swt, serpulid worm tubes.

observed at Bush Hill site (MacDonald et al., 1994; Sassen et al., 1998; Roberts et al., 1999). Thus, the ^{18}O-enriched seep carbonate may be related to the destabilization of gas hydrate. This hypothesis of the destabilization of gas hydrate providing ^{18}O-enriched water has been suggested by other studies at this site (Formolo et al., 2004), and at other cold seep sites worldwide (Bohrmann et al., 1998; Aloisi et al., 2000, 2002; Greinert et al., 2001; Chen et al., 2005).

5.1.2. Carbonate mineralogy

Authigenic carbonate precipitation at seep sites will only take place when pore fluids become sufficiently supersaturated with respect to a carbonate phase, and crystallization is not inhibited by kinetic factors (Burton, 1993). Factors that influence carbonate mineral precipitation at hydrocarbon seep sites, including the degree of carbonate supersaturation, the concentrations of Ca and Mg, the presence of complex forming anions such as SO_4^{2-} and PO_4^{3-}, temperature, pCO_2, the degree of microbial activity, and the phylogeny of the microbes involved (Naehr et al., 2007 and references therein). Aragonite seems to be favored in more oxic environments (high SO_4^{2-}) with higher total alkalinity concentrations (Burton, 1993; Savard et al., 1996). The crystallization of Mg-calcite preferentially occurs under slightly more anoxic conditions with lower SO_4^{2-} and total alkalinity concentrations (Greinert et al., 2001). Elevated temperatures generally seem to favor aragonite precipitation, while changes in saturation state seem to have little effect (Naehr et al., 2000). Aragonite can also be formed at a very fast venting site where not all of the hydrocarbon is consumed in the sulfate reducing zone, and is oxidized aerobically in shallow sediment or even in the water column directly over the seep (Hovland et al., 1987; Terzi et al., 1994).

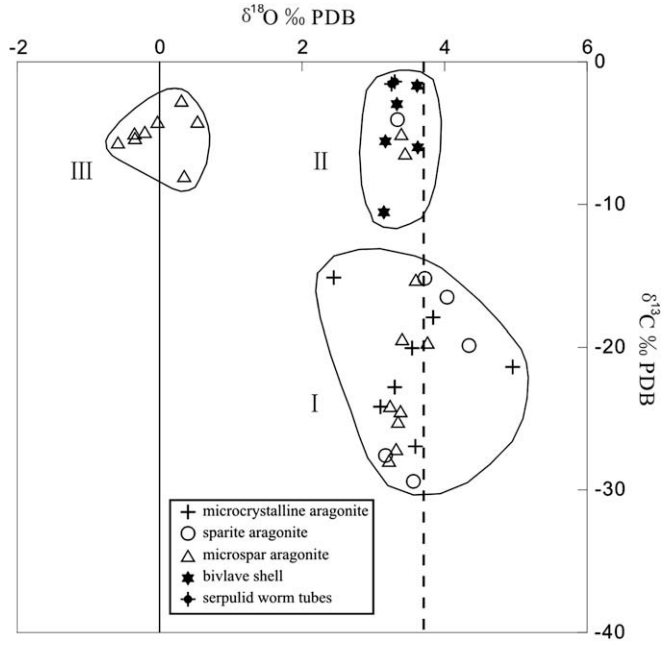

Fig. 5. Plot of $\delta^{13}C$ and $\delta^{18}O$ values of seep carbonates from Bush Hill. The dashed line represents $\delta^{18}O_{PDB}$ value (3.67‰) of aragonite precipitated in equilibrium with bottom water at 7 °C ($\delta^{18}O_{water}$ is about 0.7‰ V-SMOW).

Based on the samples analyzed in this study, the dominant mineral of the matrix of Bush Hill seep carbonate is aragonite (89–99 wt% with an average of 94 wt%, Table 1). Samples BH-C and BH-D have the highest aragonite content (up to 99 wt%), and have more pores than other samples (Fig. 2). These two samples also have the highest formation temperature based on the oxygen isotopic equilibrium calculation, suggesting that elevated temperatures seem to favor aragonite precipitation (Naehr et al., 2000). The in situ observation of temperature and gas venting flux at Bush Hill shows that higher venting rate is consistent with higher temperature (Roberts et al., 1999), suggesting that fast venting may more generally result in aragonite precipitation (Hovland et al., 1987; Terzi et al., 1994).

5.1.3. Biogenic fabrics

Evidence for an involvement of microbes in the formation of cold seep carbonates comes from stable isotopes, biomarkers, and biogenic fabrics. Pyrite occurs as framboids are often associated with authigenic carbonates, thereby indicating that sulfate reduction was active during carbonate precipitation. The association between authigenic carbonates and pyrite has already been observed in fossil seeps (Peckmann and Thiel, 2004; Campbell, 2006), and modern seeps (Aloisi et al., 2000; Sassen et al., 2004; Chen et al., 2005, 2006, 2007). Size distribution in framboids can yield insight into their genesis since rapidly-growing framboids are smaller and more homogeneous (Wilkin et al., 1996). The framboids from Bush Hill seep carbonates have an average diameter about 7 μm and are not significantly different in size.

Additional evidence for the origin of the framboidal pyrite results from its size distribution of pyrite microcrystallites within framboids. Popa et al. (2004) have shown that the size distribution of biogenic framboids have a remarkably low number of microcrystallites (10–100), which is similar to the framboids of Bush Hill seep carbonates (the number of microcrystallines could not be larger than several hundred), while most abiotic framboids contain a large number of microcrystallites (up to 10^9; Goldhaber and Kaplan, 1974).

Botryoidal aragonite is one of the typical carbonate fabrics in both modern and ancient seep carbonates (Roberts et al., 1993; Peckmann et al., 2001; Peckmann and Thiel, 2004). The botryoidal aragonite in seep carbonate usually arises from a nuclear mass of dark organic material, and was suggested to be induced by microbial activity (Roberts et al., 1993; Goedert et al., 2000). This hypothesis is in agreement with the negative stable carbon isotope values (as low as −29‰).

These biologically controlled fabrics, like clotted microfabric, botryoidal cement, and pyrite framboids preserved in seep carbonates suggest that they are being produced during methane oxidation and sulfate reduction by MOA and SRB, and those microbes are directly involved in the precipitation of authigenic carbonate at the Bush Hill gas vent site. Thus, the distinctive

Table 3
Elemental content (ppm) of 5% HNO_3-treated solution in seep carbonates samples from Bush Hill

Number	BH-A	BH-A	BH-B	BH-C	BH-C	BH-D	BH-D	BH-F	BH-F	BH-F	BH-G	BH-G	BH-H
Type[a]	mi	ar	mi	mi	ms	mi	ms	mi	ar	bi	mi	bi	mi
La	2.93	0.52	3.73	6.09	1.00	4.93	0.11	1.28	0.17	0.34	5.31	3.37	2.30
Ce	5.41	0.86	7.31	5.73	0.78	5.42	0.06	2.79	0.33	0.60	10.59	18.67	5.12
Pr	0.69	0.12	0.92	1.28	0.19	1.03	0.02	0.37	0.04	0.08	1.33	1.10	0.67
Nd	2.75	0.47	3.58	5.21	0.73	4.17	0.09	1.40	0.16	0.31	5.15	5.11	2.55
Sm	0.63	0.10	0.75	0.86	0.12	0.71	0.02	0.31	0.04	0.07	1.08	0.92	0.57
Eu	0.13	0.02	0.16	0.16	0.02	0.15	<0.01	0.07	0.01	0.02	0.24	0.17	0.08
Gd	0.53	0.09	0.58	0.54	0.10	0.51	0.02	0.28	0.04	0.07	0.94	0.68	0.51
Tb	0.09	0.01	0.09	0.09	0.01	0.08	<0.01	0.04	<0.01	0.01	0.14	0.08	0.08
Dy	0.47	0.08	0.51	0.41	0.06	0.37	0.02	0.24	0.03	0.06	0.80	0.38	0.44
Ho	0.09	0.01	0.09	0.07	0.01	0.07	<0.01	0.04	<0.01	0.01	0.15	0.06	0.08
Er	0.25	0.04	0.25	0.20	0.03	0.19	0.02	0.12	0.01	0.03	0.39	0.17	0.22
Tm	0.04	0.01	0.04	0.02	<0.01	0.02	<0.01	0.01	<0.01	<0.01	0.06	0.02	0.03
Yb	0.21	0.03	0.21	0.16	0.03	0.17	0.01	0.09	0.01	0.03	0.34	0.12	0.19
Lu	0.03	0.01	0.03	0.02	<0.01	0.02	<0.01	0.01	<0.01	<0.01	0.05	0.02	0.03
REE	14.25	2.38	18.25	20.85	3.10	17.84	0.40	7.07	0.85	1.65	26.57	30.86	12.87
Ce/Ce*	0.87	0.79	0.92	0.46	0.40	0.54	0.24	0.97	0.89	0.83	0.93	2.15	0.99
Eu/Eu*	1.10	1.14	1.18	1.13	1.03	1.17	0.99	1.05	1.00	1.09	1.12	1.04	0.70
Sc	1.66	1.31	1.99	1.66	1.07	1.51	1.16	0.05	1.17	1.20	2.64	0.06	0.04
V	19.10	5.29	16.02	13.98	4.62	14.20	0.44	7.59	3.92	2.93	28.25	6.91	5.94
Cr	9.22	3.51	7.69	4.76	2.09	4.91	1.97	0.14	2.50	2.75	7.70	0.12	0.14
Co	1.96	1.71	2.70	2.48	1.30	2.56	1.36	0.01	1.68	1.32	1.96	0.01	<0.01
Ni	9.64	9.01	13.10	13.23	11.72	17.55	7.01	0.15	12.48	7.63	11.94	0.14	0.09
Zn	12.35	3.22	14.31	6.60	3.75	6.41	8.53	0.03	15.23	2.81	9.79	0.02	0.06
As	1.95	0.26	5.29	2.94	0.85	2.32	0.05	0.33	0.18	0.05	8.50	0.51	0.25
Sr	5169	8784	7614	9147	9054	8970	2490	363	9206	2624	8678	113	94
Y	2.92	0.85	2.87	2.35	0.64	2.16	0.25	0.02	0.42	0.41	4.25	0.05	0.02
Zr	1.07	0.06	1.95	0.75	0.09	0.79	0.03	<0.01	0.11	0.03	2.61	<0.01	<0.01
Mo	1.49	1.03	2.96	0.79	0.44	0.75	0.07	0.74	1.67	1.65	6.12	0.11	0.02
Ag	0.10	0.12	0.12	0.09	0.51	0.11	0.09	0.14	0.12	0.06	0.22	0.15	0.03
Cd	0.33	0.18	1.14	0.11	0.06	0.10	0.21	0.01	0.24	0.13	0.34	<0.01	0.02
Ba	23.99	15.01	25.89	35.23	19.45	26.88	10.33	17.45	25.89	12.34	92.63	54.62	902
Hf	0.03	<0.01	0.05	0.02	<0.01	0.02	<0.01	0.01	<0.01	<0.01	0.07	0.01	0.01
Th	0.46	0.03	0.67	0.22	0.03	0.24	<0.01	0.01	0.01	0.01	1.05	0.04	0.01
U	6.25	5.94	9.93	8.30	4.20	6.95	0.10	22.48	5.31	1.01	19.83	32.04	19.42

Ce/Ce* denotes $3Ce_N/(2La_N + Nd_N)$, Eu/Eu* denotes $Eu_N/(Sm_N \times Gd_N)^{0.5}$, where N refers to normalization of concentration against the standard Post Archean Australian Shale (PAAS) (McLennan, 1989).

[a] mi, microcrystalline aragonite; ar, sparite aragonite; ms, microspar aragonite; bi, bivalve shell.

biogenic fabrics might be diagnostic markers of biogeochemical and microbiological processes at the gas vent and hydrate sites.

5.2. Ce anomaly and redox condition

The Ce anomaly provides a signal of a redox condition in contemporaneous seawater and modern oceans marked by depletion (negative anomaly) of Ce because of prevalent oxidation of Ce^{3+} to Ce^{4+} (Piper, 1974). Unlike seep carbonates from Green Canyon Block 238 and South China Sea which show no Ce anomaly (Chen et al., 2005), the shale-normalized REE patterns of the 5% HNO_3-treated solution of carbonate minerals of the Bush Hill seep carbonate show varied Ce anomalies (Table 3 and Fig. 6). The varied Ce anomalies between samples and even in the different carbonate phases in the same sample (the Ce anomaly of microcrystalline aragonite is more negative than that of sparite and microspar aragonite in the same sample, e.g. BH-G) strongly indicate the spatial and temporal change of the precipitation conditions of seep carbonate. Thus, the redox condition of seep carbonate crystallized at the Bush Hill site appears to be highly variable.

It is widely accepted that V, Mo, U, and Cd are redox sensitive elements and enriched under anoxic conditions (Morford and Emerson, 1999). Thus, they can be used to illuminate the formation condition of the carbonate. The loosely coupled relationship between the Ce anomaly and redox sensitive elements, on the other hand, indicates that the precipitation condition for Bush Hill carbonates are not simply explained (Table 3 and Fig. 6). A highly variable set of formation conditions is probable.

The variable redox conditions as well as small-scale variations in the chemical environment during carbonate precipitation may be related to microbial metabolism at seep sites. Based on the illustrations herein, we suggest that the rate of fluid flow at Bush Hill seep site may be the primary factor that controls variations in seep carbonate characteristics. During conditions of relatively slow seepage, oxidized hydrocarbon became the dominant contributing carbon source which was represented as the ^{13}C depleted carbonate (Samples BH-A, BH-B, BH-F and BH-G). At the same time, due to the slow seepage rate, carbonate precipitation occurs deep below the water/sediment interface, where being relatively anoxic, the carbonates show no or positive Ce anomalies and relatively high contents of V, Mo, U and Cd (Samples BH-A, BH-B, BH-F and BH-G). On the other hand, during the relatively high seepage, the fast seepage may force methane to be transported up to the subsurface of the seafloor, where hydrocarbons cannot be fully oxidized. Thus, the hydrocarbons become the lesser contributing carbon source which results in less negative ^{13}C signatures of the seep carbonates (Samples BH-C, BH-D and BH-H). The carbonate precipitates at subsurface or close to the water/sediment interface, where the formation condition is relatively aerobic. Thus, the carbonate precipitates here show negative Ce anomalies and relatively lower contents of V, Mo, U, and Cd (Samples BH-C, BH-D and BH-H).

6. Conclusions

Seep carbonate samples collected from the surface of the Bush Hill consist of bioclasts and matrix with variable porosity. The

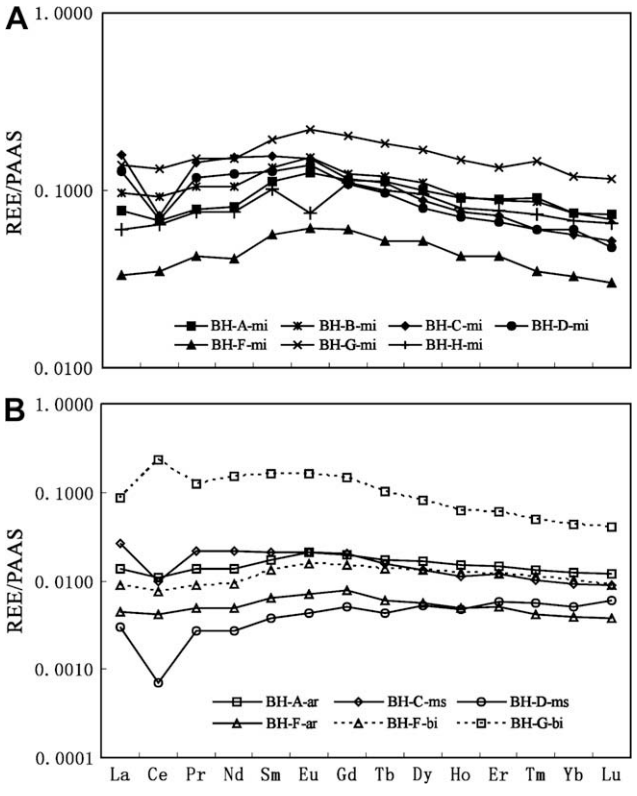

Fig. 6. Shale-normalized REE patterns of the 5% HNO_3-treated solution of seep carbonates from Bush Hill. (A) is microcrystalline aragonite (mi); (B) is sparite aragonite (ar), microspar (ms) and bivalve shell (bi).

carbonate is predominantly composed of aragonite (89–99 wt%, average 94 wt%, $n = 7$) that occurs as microcrystalline, microspar, and sparite. Pyrite framboids, clotted microfabrics, and botryoidal cements were preserved in the seep carbonates are interpreted as indicators of biologically controlled fabrics produced during microbial oxidation of hydrocarbons.

The moderately depleted $\delta^{13}C$ values ($>-29.4‰$) combined with frequent occurrences of biodegraded crude oil in the seep carbonate samples suggest that the carbon source of the seep carbonate was mainly derived from microbial degraded crude oil. The oxygen isotopic value suggests that the carbonates were precipitated from fluids at ambient bottom water. Some ^{18}O-enriched samples may be related to the destabilization of gas hydrate locally or the smectite–illite transition in deep sediments, and some ^{18}O-depleted samples may have resulted from elevated temperatures that are most probably the expulsion of warm fluids at the seafloor.

Based on the loosely coupled relationship of redox sensitive elements (V, Mo, U and Cd) and REE as well as stable isotopes and morphologies of the samples, it is suggested that the primary factor controlling or influencing the formation characteristics of seep carbonates is the flux rate of fluids and gases at the seep site. Under relatively slow seepage conditions, carbonate precipitated deep below the water/sediment interface, where conditions are anoxic and the carbonates are generally less porous and have depleted ^{13}C values. On the other hand, in relatively fast seepage settings, carbonate precipitated at shallower subsurface and even near the water/sediment interface, where the formation condition is aerobic, and the resulting carbonate occurs as more porous and with relatively less depleted ^{13}C values.

This study has examined only limited samples from a specific site. Therefore, our conclusions may be reflective of localized conditions. Notwithstanding these limitations, the data suggest that there are variable/complex formation conditions for Bush Hill seep carbonate. Through more measurements over a larger area of the GC 185 mound, the variable/complex precipitation conditions of seep carbonates may be further verified.

Acknowledgments

This study was partially supported by the National Science Foundation of China (Grants: 40725011 and U0733003), the Knowledge Innovation Program of the Chinese Academy of Sciences (Grant: KZCX2-YW-108) and the Open Fund of the Key Laboratory of Marine Geology and Environment of CAS (Grant: MGE2007KG05). The seep carbonates were obtained from the field cruises sponsored by the Minerals Management Service through a cooperative agreement (Contract No. 14-35-0001-30660) with the Coastal Marine Institute at Louisiana State University. Dr. Xuanfeng Xu (Stevens Institute of Technology, USA) helped with the quantification of XRD. Dr. Liang Qi (Institute of Geochemistry, CAS, China) helped with the analysis of trace element. Dr. Guofu Xu (Central South University, China) helped with the SEM observations. Editor D.G. Roberts and an anonymous reviewer are thanked for their careful and constructive review.

References

Aharon, P., Schwarcz, H.P., Roberts, H.H., 1997. Radiometric dating of submarine hydrocarbon seeps in the Gulf of Mexico. Geological Society of America Bulletin 109, 568–579.

Aloisi, G., Pierre, C., Rouchy, J.M., Foucher, J.P., Woodside, J., 2000. Methane-related authigenic carbonates of eastern Mediterranean Sea mud volcanoes and their possible relation to gas hydrate destabilization. Earth and Planetary Science Letters 184, 321–338.

Aloisi, G., Bouloubassi, I., Heijs, S.K., Pancost, R.D., Pierre, C., Damste, J.S.S., Gottschal, J.C., Forney, L.J., Rouchy, J., 2002. CH4-consuming microorganisms and the formation of carbonate crusts at cold seeps. Earth and Planetary Science Letters 203, 195–203.

Anderson, T.F., Arthur, M.A., 1983. Stable isotopes of oxygen and carbon and their application to sedimentologic and paleoenvironmental problems. In: Arthur, M.A., Anderson, T.F., Kaplan, I.R., Veizer, J. (Eds.), Stable Isotopes in Sedimentary Geology. Society of Economic Paleontologists and Mineralogists, Dallas, pp. 1–151.

Barrat, J.A., Boulegue, J., Tiercelin, J.J., Lesourd, M., 2000. Strontium isotopes and rare-earth element geochemistry of hydrothermal carbonate deposits from Lake Tanganyika, East Africa. Geochimica et Cosmochimica Acta 64, 287–298.

Boetius, A., Ravenschlag, K., Schubert, C.J., Rickert, D., Widdel, F., Gieseke, A., Amann, R., Jorgensen, B.B., Witte, U., Pfannkuche, O., 2000. A marine microbial consortium apparently mediating anaerobic oxidation of methane. Nature 407, 623–626.

Bohrmann, G., Greinert, J., Suess, E., Torres, M., 1998. Authigenic carbonates from the Cascadia subduction zone and their relation to gas hydrate stability. Geology 26, 647–650.

Burton, E.A., 1993. Controls on marine carbonate cement mineralogy: review and reassessment. Chemical Geology 105, 163–179.

Campbell, K.A., 2006. Hydrocarbon seep and hydrothermal vent paleoenvironments and paleontology: Past developments and future research directions. Palaeogeography, Palaeoclimatology, Palaeoecology 232, 362–407.

Chen, D.F., Cathles, L.M., 2003. A kinetic model for the pattern and amounts of hydrate precipitated from a gas steam: application to the Bush Hill vent site Green Canyon Block 185, Gulf of Mexico. Journal of Geophysics Research 108, 2058, doi:10.1029/2001JB001597.

Chen, D.F., Cathles, L.M., Roberts, H.H., 2004. The geochemical signatures of variable gas venting at gas hydrate sites. Marine and Petroleum Geology 21, 317–326.

Chen, D.F., Huang, Y.Y., Yuan, X.L., Cathles, L.M., 2005. Seep carbonates and preserved methane oxidizing archaea and sulfate reducing bacteria fossils suggest recent gas venting on the seafloor in the Northeastern South China Sea. Marine and Petroleum Geology 22, 613–621.

Chen, D.F., Feng, D., Su, Z., Song, Z.G., Chen, G.Q., Cathles, L.M., 2006. Pyrite crystallization in seep carbonates at gas vent and hydrate site. Materials Science and Engineering: C 26, 602–605.

Chen, D.F., Liu, Q., Zhang, Z., Cathles, L.M., Roberts, H.H., 2007. Biogenic fabrics in seep carbonates from an active gas vent site in Green Canyon Block 238, Gulf of Mexico. Marine and Petroleum Geology 24, 313–320.

Davidson, D.W., Leaist, D.G., Hesse, R., 1983. Oxygen-18 enrichment in the water of a clathrate hydrate. Geochimica et Cosmochimica Acta 47, 2293–2295.

Formolo, M.J., Lyons, T.W., Zhang, C., Kelley, C., Sassen, R., Horita, J., Cole, D.R., 2004. Quantifying carbon sources in the formation of authigenic carbonates at gas hydrate sites in the Gulf of Mexico. Chemical Geology 205, 253–264.

Goedert, J.L., Peckmann, J., Reitner, J., 2000. Worm tubes in allochthonous cold seep carbonates from Lower Oligocene rocks of western Washington. Journal of Paleontology 74, 992–999.

Goldhaber, M.B., Kaplan, I.R., 1974. The sulfur cycle. In: Goldberg, E.D. (Ed.), The Sea, Vol. 5. John Wiley and Sons, New York, pp. 569–655.

Greinert, J., Bohrmann, G., Suess, E., 2001. Gas hydrate-associated carbonates and methane-venting at Hydrate Ridge: classification, distribution, and origin of authigenic lithologies. In: Paull, C.K., Dillon, W.P. (Eds.), Natural Gas Hydrates: Occurrence, Distribution and Detection. Geophysical Monographs, vol. 124. American Geophysical Union, Washington, DC, pp. 131–143.

Hesse, R., Harrison, W.E., 1981. Gas hydrates (clathrates) causing pore-water freshening and oxygen isotope fractionation in deep-water sedimentary sections of terrigenous continental margins. Earth and Planetary Science Letters 55, 453–462.

Hesse, R., 2003. Pore water anomalies of submarine gas-hydrate zone as tool to assess hydrate abundance and distribution in subsurface: what have we learned in the past decade? Earth-Science Reviews 61, 149–179.

Hinrichs, K.U., Hayes, J.M., Sylva, S.P., Brewer, P.G., DeLong, E.F., 1999. Methane-consuming archaebacteria in marine sediments. Nature 398, 802–805.

Hovland, M., Talbot, M.R., Qvale, H., Olaussen, S., Aasberg, L., 1987. Methane-related carbonate cements in pockmarks of the North Sea. Journal of Sedimentary Petrology 57, 881–892.

Hudson, J.C., Anderson, T.F., 1989. Ocean temperatures and isotopic compositions through time. In: Clarkson, E.N.K., Curry, G.B., Rolfe, W.D.I. (Eds.), Environments and Physiology of Fossil Organisms. Transactions Royal Society of Edinburgh: Earth Sciences, vol. 80, pp. 183–192.

Joye, S.B., Boetius, A., Orcutt, B.N., Montoya, J.P., Schulz, H.N., Erickson, M.J., Lugo, S.K., 2004. The anaerobic oxidation of methane and sulfate reduction in sediments from Gulf of Mexico cold seeps. Chemical Geology 205, 219–238.

Leifer, I., MacDonald, I., 2003. Dynamics of the gas flux from shallow gas hydrate deposits: interaction between oily hydrate bubbles and the oceanic environment. Earth and Planetary Science Letters 210, 411–424.

MacDonald, I.R., Boland, G.S., Baker, J.S., Brooks, J.M., Kennicutt II, M.C., Bidigare, R.R., 1989. Gulf of Mexico chemosynthetic communities II: spatial distribution of seep organisms and hydrocarbons at Bush Hill. Marine Biology 101, 235–247.

MacDonald, I.R., Guinasso, N.L., Sassen, R., Brooks, J.M., Lee, L., Scott, K.T., 1994. Gas hydrate that breaches the sea floor on the continental slope of the Gulf of Mexico. Geology 22, 699–702.

MacDonald, I.R., Bender, L.C., Vardaro, M., Bernard, B., Brooks, J.M., 2005. Thermal and visual time-series at a seafloor gas hydrate deposit on the Gulf of Mexico slope. Earth and Planetary Science Letters 233, 45–59.

Matsumoto, R., 2000. Methane hydrate estimates from the chloride and oxygen isotopic anomalies. Examples from the Blake Ridge and Nankai Trough sediments. Annals of the New York Academy of Sciences 912, 39–50.

McLennan, S.M., 1989. Rare earth elements in sedimentary rocks: influence of provenance and sedimentary processes. In: Lipin, B.R., McKay, G.A. (Eds.), Geochemistry and Mineralogy of Rare Earth Elements. Reviews in Mineralogy 21, pp. 169–200.

Michaelis, W., Seifert, R., Nauhaus, K., Treude, T., Thiel, V., Blumenberg, M., Knittel, K., Gieseke, A., Peterknecht, K., Pape, T., Boetius, A., Amann, R., Jorgensen, B.B., Widdel, F., Peckmann, J., Pimenov, N.V., Gulin, M.B., 2002. Microbial reefs in the Black Sea fueled by anaerobic oxidation of methane. Science 297, 1013–1015.

Morford, J.L., Emerson, S., 1999. The geochemistry of redox sensitive trace metals in sediments. Geochimica et Cosmochimica Acta 63, 1735–1750.

Naehr, T.H., Rodriguez, N.M., Bohrmann, G., Paull, C.K., Botz, R., 2000. Methane derived authigenic carbonates associated with gas hydrate decomposition and fluid venting above the Blake Ridge Diapir. In: Paull, C.K., Matsumoto, R., Wallace, P.J., Dillon, W.P. (Eds.), Proceedings of the Ocean Drilling Program. Scientific Results 164, pp. 285–300.

Naehr, T.H., Eichhubl, P., Orphan, V.J., Hovland, M., Paull, C.K., Ussler III, W., Lorenson, T.D., Greene, H.G., 2007. Authigenic carbonate formation at hydrocarbon seeps in continental margin sediments: A comparative study. Deep-sea Research Part II 54, 1268–1291.

Peckmann, J., Thiel, V., 2004. Carbon cycling at ancient methane-seeps. Chemical Geology 205, 443–467.

Peckmann, J., Reimer, A., Luth, U., Hansen, B.T., Heinicke, C., Hoefs, J., Reitner, J., 2001. Methane-derived carbonates and authigenic pyrite from the northwestern Black Sea. Marine Geology 177, 129–150.

Piper, D.Z., 1974. Rare earth elements in the sedimentary cycle: A summary. Chemical Geology 14, 285–304.

Popa, R., Kinkle, B.K., Badescu, A., 2004. Pyrite Framboids as Biomarkers for Iron-Sulfur Systems. Geomicrobiology Journal 21, 193–206.

Qi, L., Gregoire, D.C., 2000. Determination of trace elements in 26 Chinese geochemistry reference materials by inductively coupled plasma mass spectrometry. Geostandard Newsletter 24, 51–63.

Qi, L., Zhou, M., Malpas, J., Sun, M., 2005. Determination of rare earth elements and Y in ultramafic rocks by ICP-MS after preconcentration using $Fe(OH)_3$ and $Mg(OH)_2$ coprecipitation. Geostandards and Geoanalytical Research 29, 131–141.

Roberts, H.H., 2001. Fluid and gas expulsion on the Northern Gulf of Mexico continental slope: mud-prone to mineral-prone responses. In: Paull, C.K., Dillon, W.P. (Eds.), Natural Gas Hydrates: Occurrence, Distribution, and Detection. American Geophysical Union, Washington, DC, pp. 145–161.

Roberts, H.H., Aharon, P., 1994. Hydrocarbon-derived carbonate buildups of the northern Gulf of Mexico continental slope: A review of submersible investigations. Geo-Marine Letters 14, 135–148.

Roberts, H.H., Aharon, P., Walsh, M.M., 1993. Cold-seep carbonates of the Louisiana continental slope-to-basin floor. In: Rezak, R., Lavoie, D.L. (Eds.), Carbonate Microfabrics. Springer, Berlin, pp. 95–104.

Roberts, H., Wiseman Jr., W., Hooper, J., Humphrey, G.D., 1999. Surficial gas hydrates of the Louisiana continental slope-initial results of direct observations and in situ data collection. Offshore Technology Conference, Houston, TX, pp. 259-272.

Sackett, W.M., 1978. Carbon and hydrogen isotope effects during the thermocatalytic production of hydrocarbons in laboratory simulation experiments. Geochimica et Cosmochimica Acta 42, 571–580.

Sassen, R., MacDonald, I.R., Guinasso Jr., N.L., Joye, S., Requejo, A.G., Sweet, S.T., Alcala-Herrera, J., DeFreitas, D.A., Schink, D.R., 1998. Bacterial methane oxidation in sea-floor gas hydrate: significance to life in extreme environments. Geology 26, 851–854.

Sassen, R., Milkov, A.V., Ozgul, E., Roberts, H.H., Hunt, J.L., Beeunas, M.A., Chanton, J.P., DeFreitas, D.A., Sweet, S.T., 2003. Gas venting and subsurface charge in the Green Canyon area, Gulf of Mexico continental slope: evidence of a deep bacterial methane source? Organic Geochemistry 34, 1455–1464.

Sassen, R., Roberts, H.H., Carney, R., Milkov, A.V., DeFreitas, D.A., Lanoil, B., Zhang, C., 2004. Free hydrocarbon gas, gas hydrate, and authigenic minerals in chemosynthetic communities of the northern Gulf of Mexico continental slope: relation to microbial processes. Chemical Geology 205, 195–217.

Savard, M.M., Beauchamp, B., Veizer, J., 1996. Significance of aragonite cements around Cretaceous marine methane seeps. Journal of Sedimentary Research 66, 430–438.

Sholkovitz, E., Shen, G.T., 1995. The incorporation of rare earth elements in modern coral. Geochimica et Cosmochimica Acta 59, 2749–2756.

Taylor, J.C., 1991. Computer Programs for Standardless Quantitative Analysis of Minerals Using the Full Powder Diffraction Profile. Powder Diffraction 6, 2–9.

Terzi, C., Lucchi, F.R., Vai, G.B., Aharon, P., 1994. Petrography and stable isotope aspects of cold-vent activity imprinted on Miocene-age "calcari aLucina" from Tuscan and Romagna Apennines, Italy. Geo-Marine Letters 14, 177–184.

Tryon, M.D., Brown, K.M., 2004. Fluid and chemical cycling at Bush Hill: Implications for gas and hydrate-rich environments. Geochemistry Geophysics Geosystems 5, 12004.

Valentine, D.L., Reeburgh, W.S., 2000. New perspectives on anaerobic methane oxidation. Environmental Microbiology 2, 477–484.

Whiticar, M.J., Faber, E., Schoell, M., 1986. Biogenic methane formation in marine and freshwater environments: CO_2 reduction vs. acetate fermentation-Isotope evidence. Geochimica et Cosmochimica Acta 50, 693–709.

Wilkin, R.T., Barnes, H.L., Brantley, S.L., 1996. Pyrite formation by reactions of iron monosulfides with dissolved inorganic and organic sulfur species. Geochimica et Cosmochimica Acta 60, 4167–4179.